Science of the Total Environment 875 (2023) 162682

Contents lists available at ScienceDirect

Science of the Total Environment

journal homepage: www.elsevier.com/locate/scitotenv

Rare earths release from dissolving atmospheric dust and their accumulation into crystallising halite: The Dead Sea example

P. Censi [a,*], I. Sirota [b,c], P. Zuddas [d], N.G. Lensky [b,c], O. Crouvi [b], M. Cangemi [a], D. Piazzese [a]

[a] Department of Earth and Marine Science (DISTEM), University of Palermo, Via Archirafi 36, 90123 Palermo, Italy
[b] Geological Survey of Israel, 32 Yesha'yahu Leibowitz, Jerusalem 9371234, Israel
[c] Institute of Earth Sciences, Edmond J. Safra Campus, The Hebrew University of Jerusalem, Givat Ram, Jerusalem 91904, Israel
[d] Sorbonne Université, CNRS, METIS, F75005 Paris, France

HIGHLIGHTS

- REE in Dead Sea brines are released from dissolving atmospheric dust particles.
- The halite crystallisation affects the REE distribution along the water column.
- Both these process correspond to REE extraction from their primary rock source.

GRAPHICAL ABSTRACT

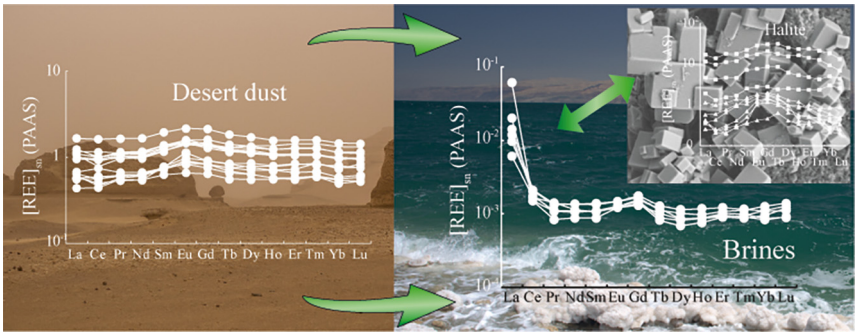

ARTICLE INFO

Editor: Filip M.G.Tack

Keywords:
Rare earth elements
Dead Sea brines
Lanthanum anomaly
Halite

ABSTRACT

The industrial extraction of Y and lanthanides (hereafter defined as Rare Earth Elements, REE) often requires the achievement of leaching procedures removing these metals from primary rocks and their transfer in aqueous leachates or incorporated in newly forming soluble solids. These procedures are the most dangerous to the environment in relation to the composition of leachates. Hence, the recognition of natural settings where these processes currently occur, represents a worthy challenge for learning how to carry out similar industrial procedures under natural and more eco-friendly conditions. Accordingly, the REE distribution was studied in the brine of Dead Sea, a terminal evaporating basin where brines dissolve atmospheric fallout particles and crystallise halite.

Our results indicate that the shale-like fractionation of shale-normalised REE patterns in brines, inherited during the dissolution of atmospheric fallout, changes because of the halite crystallisation. This process leads to crystallising halite mainly enriched in elements from Sm to Ho (medium REE, MREE) and coexisting mother brines enriched in La and some other light REE (LREE). We suggest that the dissolution of atmospheric dust in brines corresponds to the REE extraction from primary silicate rocks, whereas halite crystallisation represents the REE transfer into a secondary more soluble deposit with reduced environmental health outcomes.

1. Introduction

Rare Earths are strategic metals presently used from a wide range of electronic, chemical, and oil-refinery industries. These elements are extracted from mines exploiting primary lithogenic deposits through invasive procedures for the environment (Li, 2011; Hao et al., 2015; Gwenzi et al.,

* Corresponding author.
E-mail address: paolo.censi@unipa.it (P. Censi).

http://dx.doi.org/10.1016/j.scitotenv.2023.162682
Received 20 December 2022; Received in revised form 1 March 2023; Accepted 2 March 2023
Available online 7 March 2023

2018). Accordingly, REE are considered today an emerging new class of pollutants in relation to a wide recognition of positive Gd and La anomalies in urban and peri-urban catchments and related aquifers (Bau and Dulski, 1996; Möller et al., 2000; Kulaksiz and Bau, 2007, 2011, 2013). Dissolved REE can be involved in scavenging processes onto suitable mineral or organic surfaces (Takahashi et al., 2005, 2007, 2010; Geng et al., 2022; Wilfong et al., 2022 and references therein) or fractionate during the authigenic mineral formation despite the amplitude of this process was not recognized under natural conditions (Terakado and Masuda, 1988; Kagi et al., 1993; Qu et al., 2009a, 2009b).

Halite crystallisation was found to fractionate REE relative to the coexisting aqueous phase (Censi et al., 2017, 2020). Yet, it remains unclear the extent of this fractionation and whether it can represent a method of remediation for natural waters contaminated by high REE concentrations. To resolve this problem, we perform this study in the Dead Sea, a terminal lake with a progressively declining level in response to negative water balance (Lensky et al., 2005). The Dead Sea is divided into two main basins: The Northern Basin occupied by a deep hypersaline lake that is actively precipitating halite (Arnon et al., 2016; Kirkham et al., 2020; Lensky et al., 2005; Sirota et al., 2016, 2017, 2021) and the Southern Basin, occupied by shallower evaporation ponds, which are currently exploited for saltwork (Ganor and Katz, 1989). Here, brines are also oversaturated in carnallite, a KCl salt typical of last stages of brine evaporation (Bąbel and Schreiber, 2014).

In this study, the evolution of REE concentration in halite crystals and their mother brine are explored in two different evaporitic settings, (i) along the water column of the Dead Sea down to 66 m depth in the Northern Basin, and (ii) along the crystallisation path of carnallite in the Southern basin. Halite crystals were also analysed and the REE concentration compared with values measured in corresponding brines. Accordingly, this site is a suitable laboratory for investigating how aqueous REE attain to concentrations ten times higher than seawater and the REE contents in brines significantly reduced during the halite crystallisation.

2. Geochemical background

Rare earth elements (REE) constitute the lanthanide series from $_{57}$La to $_{71}$Lu (lanthanides) including $_{39}$Y (Shannon, 1976). They usually form trivalent ions displaying similar reactivity through aqueous processes (Cotton, 2006). The progressive filling of 4f orbital between $_{57}$La to $_{71}$Lu however, generates progressive decreasing of ionic radius along the series (Lanthanide contraction) identifying subtle differences is the geochemical reactivity usually highlighted by normalization of analytical REE concentrations (Migaszewski and Gałuszka, 2015). Here, measured REE concentrations $[REE]_{meas}$ have been normalised towards the reference concentration $[REE]_{PAAS}$ of Post Archean Australian Shale $[REE]_{PAAS}$ (Taylor and McLennan, 1985) according to:

$$[REE]_n = \frac{[REE]_{meas}}{[REE]_{PAAS}} \tag{1}$$

After normalization, REE concentrations follow a smooth trend where elemental enrichments/depletion and fractionations of groups of elements can be recognized in each natural sample. These features correspond to the above-mentioned subtle reactivity differences (Comin-Chiaramonti et al., 1991; Bau, 1996; Ruberti et al., 2002) and explained by the partial involvements of 4f electrons during the formation of donor-acceptor bonds (Löble et al., 2015; Lukens et al., 2016). These bonds are generally formed during aqueous complexation reactions or removal onto the surfaces of suspended solids. Elemental enrichments/depletions along the REE series can be measured as positive/negative anomalies according to the general expression:

$$\frac{[REE]_i}{[REE]_i^*} = \frac{2[REE]_i}{[REE]_{(i+1)} + [REE]_{(i-1)}} \tag{2}$$

where brackets are normalised REE concentrations (Alibo and Nozaki, 1999). REE* are background normalised concentrations assessed from those measured for the preceding (i-1) and following (i + 1) elements along the REE series, respectively. Since La is the first element of the series, its anomaly is assessed as follows (Alibo and Nozaki, 1999).:

$$\frac{La}{La*} = \frac{[La]_n}{3[Pr_n] + 2[Nd_n]} \tag{3}$$

When REE/REE* is >1, we have positive anomalies since the normalised concentrations of the considered elements are higher than their corresponding background values. Analogously, anomalies of elements or groups of elements with similar behaviour through geochemical process can be assessed along the REE series. Consequently, the anomaly of medium REE (MREE) corresponding to the elements from Sm to Dy can be assessed with respect to light REE (LREE) from La to Nd and to heavy REE (HREE) from Ho to Lu by the following Eq. (4) (Ding et al., 2006):

$$\delta MREE = \frac{[MREE]_n}{\sqrt{[LREE]_n * [HREE]_n}} \tag{4}$$

where [LREE], [MREE] and [HREE] are defined as follows:

$$\Sigma[LREE]_n = [La]_n + [Ce]_n + [Pr]_n + [Nd]_n \tag{5}$$

$$\Sigma[MREE]_n = [Sm]_n + [Eu]_n + [Gd]_n + [Tb]_n + [Dy]_n + [Ho]_n \tag{6}$$

$$\Sigma[HREE]_n = [Er]_n + [Tm]_n + [Yb]_n + [Lu]_n \tag{7}$$

The apparent distribution coefficient for REE incorporated in halite and assumed to substitute Na in the lattice can be calculated by:

$$D_{REE} = \frac{\left[\frac{[REE]_i}{[Na]}\right]_{halite}}{\left[\frac{[REE]_i}{[Na]}\right]_{brine}} \tag{8}$$

3. Regional settings

The Dead Sea two basins includes the northern basin, occupied by a deep (~280 m) hypersaline lake (density ~ 1245 kg m^{-3}) (Arnon et al., 2016; Sirota et al., 2016), and the southern shallow basin which operates as evaporation ponds (~2 m) for the potassium industries (Fig. 1). The division into two basins results from the continuous lake level decline below the dividing sill, as the northern remains a 'natural lake' and the southern is maintained as a series of industrial evaporation ponds (Lensky et al., 2005).

In the Dead Sea area, the lithogenic solids supply to brines was studied both in terms of deposition of atmospheric dust and continental runoff. The flux of atmospheric dust resulted high up to ~50 g m^{-2} y^{-1} (Ganor and Foner, 2001; Singer et al., 2003) and was originated both from local (Negev and Judean deserts) and "foreigner" sources (Singer et al., 2003; Kalderon-Asael et al., 2009).

Floods transported through the riverine runoff also occur besides to a lesser extent than in the past due to the progressive increase in the exploitation of water resources in surrounding areas (Nehorai et al., 2013; Palchan et al., 2018; Belmaker et al., 2019; Eyal et al., 2021). As observed in other natural areas (Penn et al., 2001; Thiagarajan and Aeolus-Lee, 2004), dust-particles supplied to the Dead Sea area often consist of a silicate nucleus coated by a mixture of clays and phosphatised Mn—Fe oxyhydroxides (Goldsmith et al., 2014; Macholdt et al., 2015, 2017). These coatings are enriched in REE, especially MREE (Thiagarajan and Aeolus-Lee, 2004). Accordingly, the dissolution of these solids in contact with natural waters results in a clear REE signature of shallowest water layers in epicontinental basins and coastal waters (Censi et al., 2005; 2007; 2019).

The northern Dead Sea basin (Fig. 1) is considered among the closest modern analogues of a hypersaline basin that deposited ancient saline giants (Bąbel and Schreiber, 2014); the deposition of halite layers can be described using the saline-model (Rouchy and Caruso, 2006; Warren, 2006) where negative water balance and water evaporation are crucial (Bąbel and Schreiber, 2014). In the Dead Sea, halite has been actively precipitated

during the last four decades in response to a negative water balance (Steinhorn, 1983; Levy, 1992; Anati, 1993; Gavrieli, 1997; Sirota et al., 2016, 2017, 2018, 2020, 2021). The low water activity (<0.65) of the Dead Sea brines (Salhotra et al., 1987; Lensky et al., 2018; Mor et al., 2018) prevents significant biological activity and biogenic particulates (Bodaker et al., 2010) and the sparsely populated surroundings contribute minor input of anthropogenic solids (Al-Hanbali and Kondoh, 2008). The behaviour of REE in these strong electrolyte solutions results from authigenic inorganic reactions along the water column without any significant biological or anthropogenic input. Dead Sea is thus a suitable site for reconstructing the evolution of REE distribution in evaporating brines under effects of authigenic processes. We have sampled brines and halite crystals offshore (Fig. 1), during a period with no floods, though the lithogenic input most likely originated from direct atmospheric fallout.

REE concentrations were analysed in the Northern Dead Sea brines following selected sampling cruises or spot sampling between 1993 and 2018 (Gavrieli and Halicz, 2002; Censi et al., 2020). REE analyses were carried out also in halite crystals collected along the shoreline and through the Northern Dead Sea water column (Censi et al., 2017, 2020).

The evaporation ponds in the southern basin are fed by pumping brines from the northern basin (Fig. 1). The first pond is occupied by the brine of the northern basin and from there the salinity of each pond increases along an evaporation path concurrently with halite precipitation (the path of brines is represented by arrows in Fig. 1). Since the REE composition in atmospheric dust and source rocks from desert areas is closely similar (Macholdt et al., 2017), possible changes of REE composition in brines should be provided by the salt crystallisation along an evaporation path.

4. Methods

4.1. Sampling

Brine samples from the northern basin were collected offshore En-Gedi (EG; Fig. 1). Coupled salt samples and their mother brines were collected

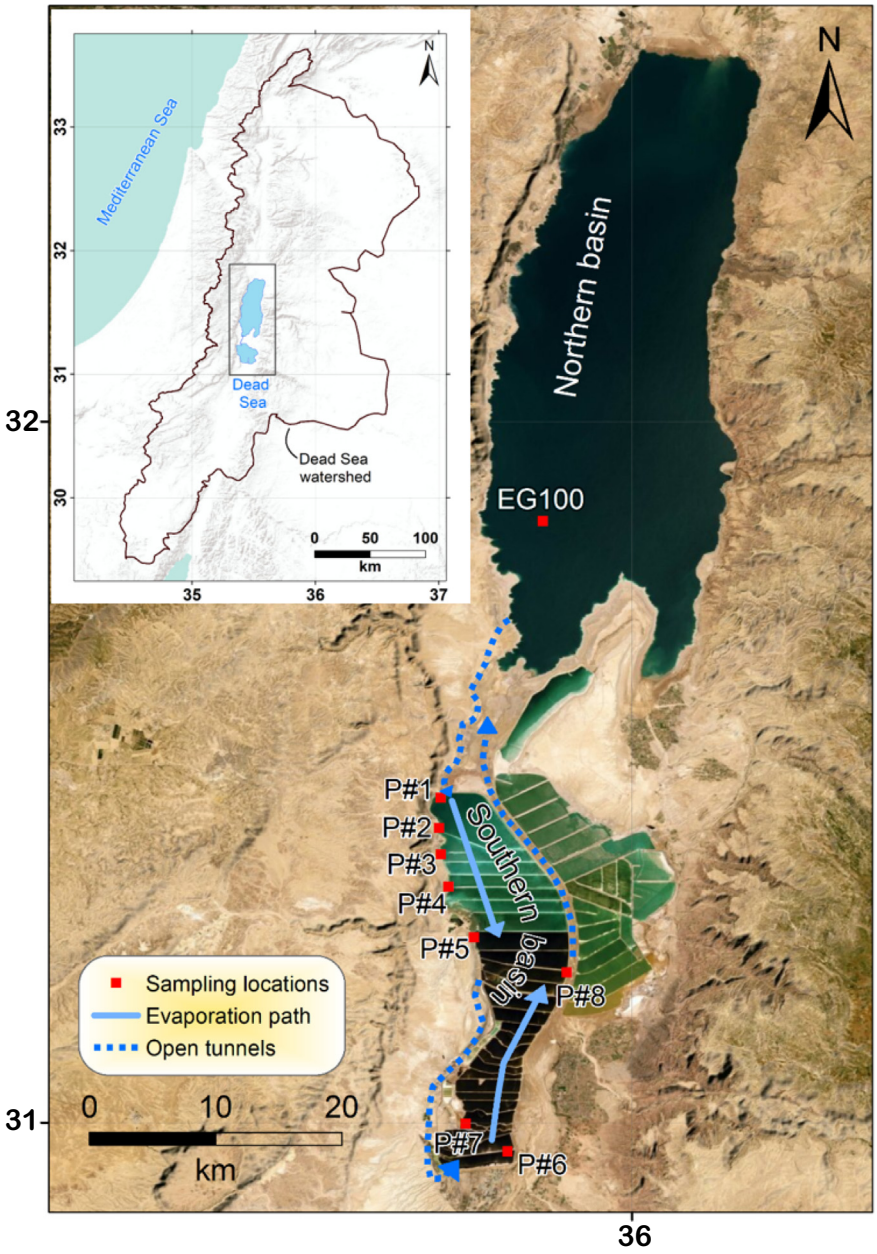

Fig. 1. The Dead Sea area with the location of sampling sites.

from depths of 1 to 66 m at the oceanographic buoy EG-100 (31.429 N, 35.435E; November 27, 2019) using the R/V Taglit.

Salt samples were collected from a steel cable that was submerged along the water column and crystalized halite along it (Sirota et al., 2016). Brine samples were collected using Niskin bottles (General Oceanic, 1080 2.7 L, Miami, FL, USA) at the depths where the salt samples were collected.

Coupled salt samples and their mother brines from the southern basin were collected from different ponds along the path of evaporation, at the shoreline of each pond, as depicted in Fig. 1. A brine sample was collected from the feeding channel delivering brines from the northern basin (P#1 sampling site, Fig. 1).

4.2. Analytical procedure

Two litres of brine were collected at each sampling depth, diluted 1:2 to avoid salt crystallisation, and then stored in previously cleaned polyethene bottles. After 2 h, samples were filtered in the lab (Millipore™ manifold filter, diameter 47 mm, pore size 0.45 μm) then 5 % HNO_3 ultrapure acid solution was added to attain pH ≈ 2.

Halite crystals were collected from the cable at the same depth of brines along the Dead Sea water column. After the removal of crystals in contact with the cable, an aliquot of clean crystals was collected in a clean vial for analysis. Crystals were studied both washed and unwashed to assess the extent of the removal of studied elements both in the adsorbed fraction and incorporated in the halite crystal. In the laboratory, some crystals were thoroughly washed in ultrapure water and dried at 50 °C (Herut et al., 1998) and identified as 'washed halite'. Other crystals from each sample were stored unwashed in precleaned vials and identified as 'unwashed halite'. A 0.5 g aliquot of each sample was dissolved in 1 L of 5 % HNO_3 acid solution then stored in a previously cleaned polyethylene bottle.

The major element concentration in brines was measured by two Dionex ionic chromatographs: one equipped with a CS-12A column to determine cations (Na, K, Mg, and Ca) and another equipped with an AS-14A column to analyse anions (Cl-, SO_4^{2-}). Alkalinity was determined by titration with 0.1 N HCl. Major element concentration was used only to assess the salinity of brines and calculate their Na/Cl molar ratio.

REE concentrations in brines and solutions representative of halite crystals and salt minerals were analysed according to Raso et al. (2013). An excess of $FeCl_3$ (1 %) solution is added to each sample (1 L) and then followed by a suitable volume of NH_4OH (25 %) solution to attain a pH of 8 inducing the precipitation of solid $Fe(OH)_3$. Accordingly, REE are scavenged onto the surface of the crystallising solid and then separated the aqueous phase by filtration. The yield of $Fe(OH)_3$ crystallisation was always higher than 95 %. Precipitated $Fe(OH)_3$ was collected on a membrane filter (Millipore™ manifold filter, diameter 47 mm, pore size 0.45 μm). Then, the solid filtrate was dissolved in 3 M HCl and the obtained solution diluted to 1 M and analysed by Quadrupole-ICP-MS (Agilent 7500 series equipped with a collision cell). All water and halite samples were processed in a laminar flow clean bench to minimise contamination, and all sampling materials were previously cleaned with high purity grade reagents (Baker Ultrex II®). All materials used to collect and manipulate water samples were plasticware and were cleaned by acid with 1:10 hot high purity HNO_3 solutions. The overall procedure and a detailed evaluation of the analytical errors are reported in Raso et al. (2013).

According to Raso et al. (2013), both samples and calibration standards were prepared in the same HCl 1 M medium. The ICP-MS instrument used for analyses was tuned with a solution containing 1 ng mL^{-1} of Ce and Ba in

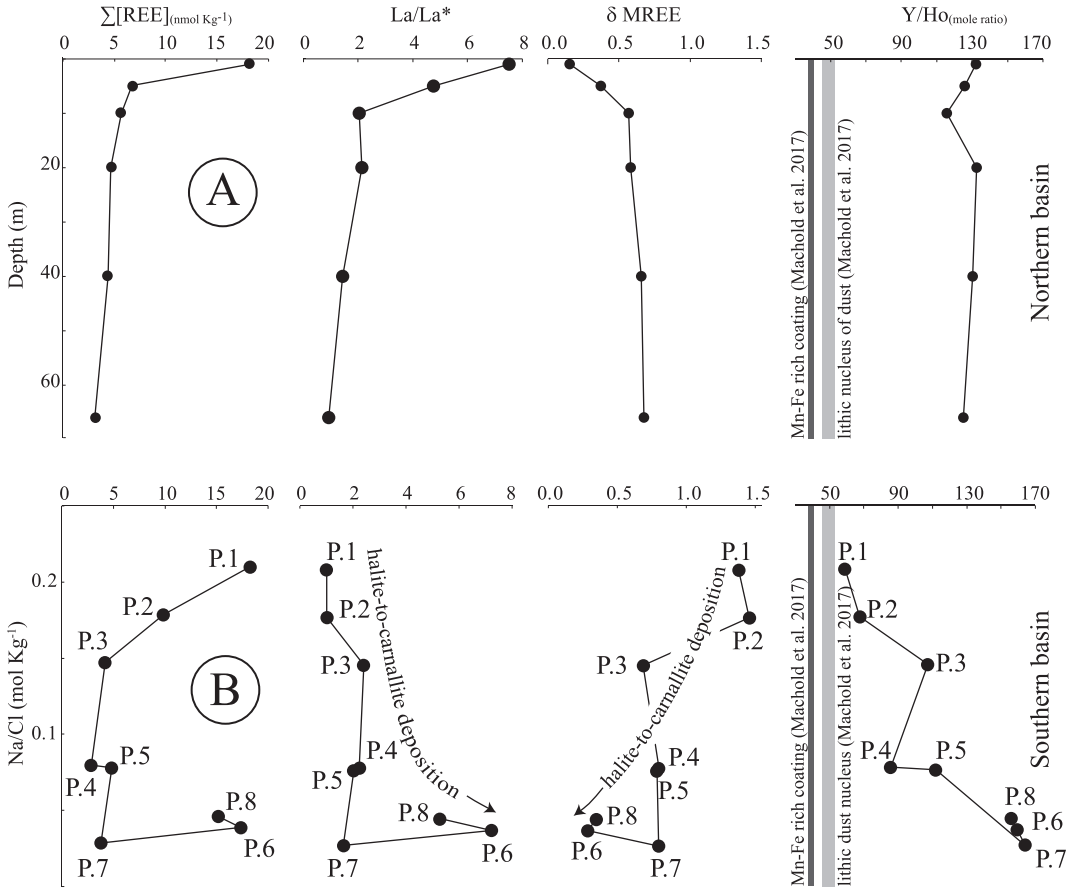

Fig. 2. The overall REE concentration, La/La*, δMREE, and Y/Ho values reported versus depth in northern lake brines (A) and versus Na/Cl molar ratio in southern pond brines (B). The range of Y/Ho values in the Fe—Mn coating and lithic nucleus of dust particles are reported for reference (Macholdt et al., 2017). Error bars are within the size of the symbols.

a HCl 1 M medium. Consequently, the extent of spectral interferences due to the formation of Ce-Ba-Cl-O-OH-H charged species was assessed resulting not higher than 5 %. Each solution was analysed three times with a classical external calibration mode. Further indications of analytical procedures are detailed in Raso et al. (2013).

All chemicals used during laboratory manipulations were of ultrapure grade. Ultrapure water (resistivity of 18.2 MΩ cm or better) was obtained from an Arium® mini system (Sartorius, Italy). Nitric acid 65 % (*w*/w), ammonia solution and hydrochloric acid were purchased from J.T. Baker chemicals. Working standard solutions of the studied elements were prepared daily by stepwise dilution of the multi-element stock standard solutions from DBH, Merck or CPI International (1000 ± 5 mg L^{-1}) in a 1 M HCl medium. All labware was polyethylene, polypropylene or Teflon and the calibration of all volumetric equipment was verified. The assessment of the analytical precision was carried out by analysing five aliquots (500 mL each) of NASS-6 (seawater certified reference material for trace metals) distributed by the National Research Council of Canada. These were treated as water samples according to the above-mentioned procedure and the obtained concentrations compared with those previously reported by Raso et al. (2013) and Lemaitre et al. (2014). Obtained values are reported in Table S1 of the Supporting Information.

Table S1 shows that La, Ce, Nd and Y values are those affected by the larger uncertainty (4, 3, 5 and 9 pmol Kg^{-1}, respectively). Table S2 and S3 of the Supporting Information also show that La, Ce, Nd and Y concentrations measured in brines and halite crystals are reported in nmol Kg^{-1}, and μmol Kg^{-1}, respectively. Accordingly, the measured uncertainties resulting from the analytical procedure of REE preconcentration from brines and crystals should have a limited influence on the measure of REE concentration in these materials.

5. Results

The concentration of REE in brines from both northern and southern basins is reported in Table S2 of Supporting Information, while REE concentrations measured in corresponding halite crystals are reported in Table SI-3 of Supporting Information.

5.1. Northern basin

In the northern part of the Deed Sea, the overall REE concentration decreases by 18.9 to 3.7 nmol Kg^{-1} from the surface to the bottom respectively. (Fig. 2A). In these waters, we found that (La/La)* sharply decreases from 7.6 (at the surface layers) to 2.0 after 10-m depth while the δMREE increases from 0.2 and 0.7 along the water column. The Y/Ho molar ratio decreases from 132.7 to 115.6 in the first 10 m reaching the constant value of 132 from 15 m to the bottom. The ratios observed in this part of the basin are higher when compared to that of crustal materials and chondrites (Jochum et al., 1986) indicating possible atmospheric contribution from dust-particle dissolution.

In this region, dust-particles are mainly constituted by lithogenic materials characterised by coatings made of iron oxyhydroxides phases (Goldsmith et al., 2014; Macholdt et al., 2015) as additional anthropogenic source can be excluded given the very low density of urban and industrial activities.

Unwashed halite crystals have the overall REE concentration higher compared to the washed crystals. Unwashed halite crystals have positive La and MREE anomalies in agreement with the observed positive La anomaly of all sampled brines suggesting possible La adsorption from the La-enriched brines onto the surface of unwashed halite crystals. The La and MREE anomalies are not found in the washed halite crystals.

5.2. Southern basin

In the southern basin, brines have Na/Cl molar ratio ranging from 0.2 to 0.03 throughout the different ponds (Fig. 1). Here, brines arrive from Northern basin and change the halite oversaturation favouring the formation of carnallite, a typical KCl salt of evaporating conditions found in the 8th pond (sample P#8, Fig. 2B). We found that changing of the neogenic

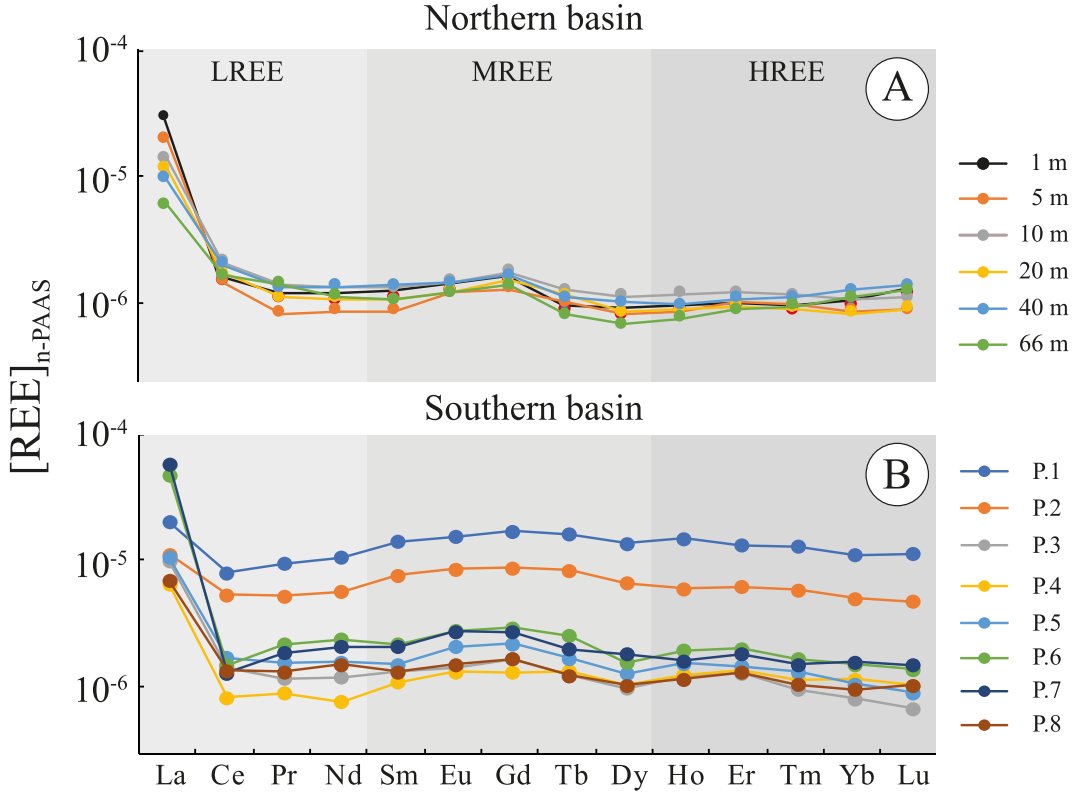

Fig. 3. Shale-normalised REE concentrations in brines from the northern (A) and southern basins (B). Shaded areas group elements from LREE, MREE, and HREE.

mineral formation (i.e. halite versus carnallite,) produce a change of the REE behaviour. Indeed, the Σ[REE] progressively decreases until sample P.7, then suddenly increases and that both La/La* and δMREE span from 0.4 to 6.5 and from 1.4 to 0.3, respectively as results of the halite versus carnallite mineral formation. The Y/Ho molar ratio progressively rises from 59.4 (feeding brine) to 162.7 along the halite-to-carnallite mineral changing. Fig. 3B shows strong positive La anomalies especially in P#6 and P#7 samples and lower δMREE. This may reflect the removing of MREE from brines during the crystallisation of potassic salts. The crystallisation of carnallite also produce an increase of the mass fraction of solids in brines. Since Ho usually shows a larger affinity towards surfaces than Y during rock-water interactions (Bau and Dulski, 1999; Qu et al., 2009a, 2009b; Censi et al., 2017, 2020), the Ho fractionation onto carnallite surfaces relative to Y could favour the Y/Ho molar ratio increasing as observed in the last ponds.

6. Discussion

We found that REE in the Dead Sea basin appear depending on two major processes, (i) the dissolution of dust particle with an average REE concentration close to 137 mg Kg^{-1} (Goldsmith et al., 2014; Palchan et al., 2018), and (ii) the processes of adsorption and incorporation of REE during the halite formation through the water column. If the REE concentration in shallow waters of the northern basin reflects the atmospheric particle dissolution and given the lake surface area of ~600 km^2 (Sirota et al., 2016), the potential amount of REE delivered to brines is by 4×10^3 tons/years.

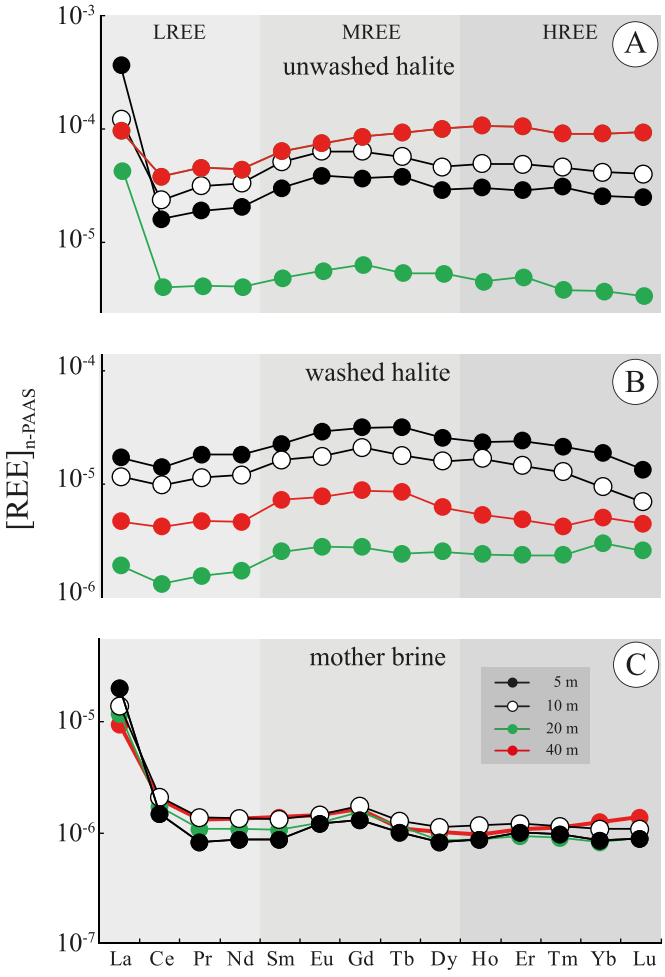

Fig. 4. Shale-normalised REE concentrations measured in unwashed halite (A), washed halite crystals (B), and mother brines (C). Shaded areas group elements from LREE, MREE, and HREE.

The observed progressive drop of REE concentration along the water column reflects the progressive removing of about 85 % of these dissolved elements by the formation of halite crystals. In the case of the Y/Ho ratio, the dissolution of atmospheric lithogenic particles should produce brines with constant Y/Ho ratio (Goldsmith et al., 2014; Macholdt et al., 2015; Palchan et al., 2018; Censi et al., 2017). The observed variation of Y/Ho molar ratio may correspond to preferential removal of Ho relative to Y in strong electrolyte conditions (Qu et al., 2009a, 2009b; Censi et al., 2017, 2018, 2020). Since Fe oxyhydroxide coatings on atmospheric particles have subchondritic Y/Ho molar ratio (Goldsmith et al., 2014; Macholdt et al., 2015; Palchan et al., 2018), their dissolution generates lower Y/Ho ratios in the upper water column compared to the bottom where lithic nuclei of atmospheric particles are already dissolved.

Our study reveals that halite crystals preferentially retain MREE rather that LREE, as identified in the shale-normalised REE pattern of washed halite crystals of Fig. 4B. This behaviour agrees with the Goldschmidt's rules (Goldschmidt, 1937) and previous trace metal ions behaviour as they easily substitute in the lattice other major elements having closer ionic radii (Censi et al., 2017, 2020). During the halite crystallisation, the lanthanide contraction of ionic radii for elements along the REE series makes possible the REE substitution in the sodium position of the lattice (Censi et al., 2020). Since Eu^{3+} has ionic radius closer to Na^+ (Shannon, 1976) substitution in halite crystals is enhanced with respect to other REE likes La^{3+} (Censi et al., 2020) explaining the observed positive lanthanum anomaly found in the unwashed crystals. Since La^{3+} is poorly incorporated in halite lattice, brines could have higher La/La* compared to halite as observed in our study.

In the Dead Sea we have shown that dissolution of atmospheric dust controls the initial REE concentration $[REE]_i$ of brines while the observed changing should result to the process of halite crystallisation, throughout a possible process of co-precipitation. Assuming that during the halite formation the layer of deposit solid do not participate to the reaction after

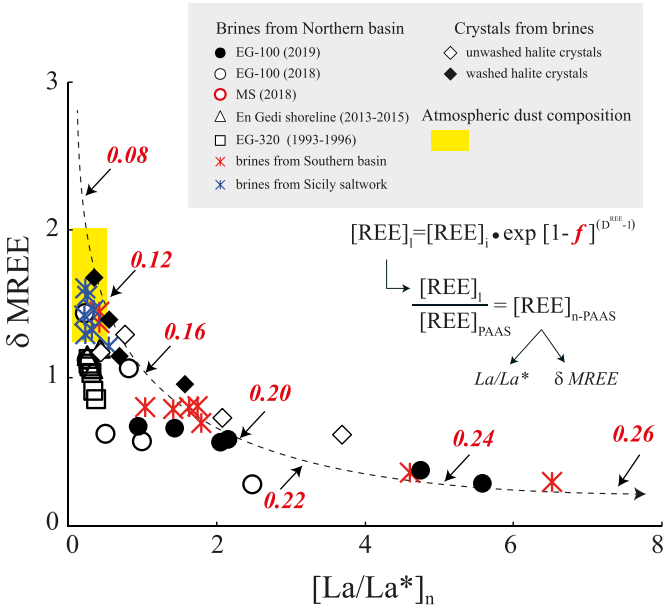

Fig. 5. La/La* and δMREE values from northern and southern Dead Sea basins compared with reference data from the northern Dead Sea basin between 1993 and 2018 and Sicily saltwork (Gavrieli and Halicz, 2002; Censi et al., 2017, 2020). Values measured in washed and unwashed halite crystals are also reported. The yellow dashed area corresponds to the composition of atmospheric dust falling on the Dead Sea basin. Red bold numbers along the curved trend correspond to the fraction of crystallised halite (*f* value in Eq. (8)). The flow chart illustrating how La/La* and δMREE values are assessed from Eq. (8) is also reported.

deposition and that the superficial layer is in equilibrium with the brines, the process could follow the Doerner and Hoskins (1925) law by:

$$[REE]_l = [REE]_i * [1 - f]^{(D_{REE} - 1)} \quad (9)$$

where f corresponds to the fraction of crystallising halite and D is the distribution coefficient of REE between brines and halite.

Eq. (9) corresponds to the role provided by halite crystallisation on the changing of REE concentration in brines from the initial REE concentration $[REE]_i$ to a given $[REE]_l$ value as a function of the mass fraction f of crystallising halite ($0 \leq f \leq 1$) and the (apparent) distribution coefficient of REE, D_{REE}. Normalising this set of $[REE]_l$ values according to Eq. (1), a corresponding set of normalised $[REE]_n$ concentrations were obtained where every $[REE]_n$ concentration is given by the sequence of normalised concentrations from $[La]_n$, to $[Lu]_n$ that can be used to assess La/La* and δMREE values according to Eqs. (3) and (4), respectively. Using $[REE]_i$ and $D_{REE,}$ the composition of Dead Sea brines and distribution coefficient of REE measured in 2015 during the halite crystallisation (Censi et al., 2017) respectively, the change of the mass fraction of crystallising halite f between 0 and 0.26 results in a set of $[REE]_l$ values from Eq. (9). Normalising these $[REE]_l$ values to PAAS, a resulting set of La/La* and δMREE values are assessed and displayed in Fig. 5 where La/La* and δMREE values obtained from this study are compared with those resulting from previous Dead Sea studies (Gavrieli and Halicz, 2002; Censi et al., 2017, 2020) and brines from a saltwork (Censi et al., 2017). We also reported values corresponding to REE concentrations measured in atmospheric dust currently deposed over the Dead Sea surface (Goldsmith et al., 2014; Palchan et al., 2018). We found that La/La* and δMREE from brines of saltwork closely fall to the atmospheric dust composition since the brine collection was carried out during the winter and halite crystallisation does not takes place at the period. Fig. 5 also shows that La/La* and δMREE values from washed halite crystals fall close to the composition of atmospheric dust particles, whereas unwashed samples follow a trend like brines. Since MREE are those elements of REE series with closest ionic radii to that of Na^+, washed halite fractionate MREE leaving La and other elements of the REE series enriched in mother brines. In unwashed crystals, where small amounts of brine remain adsorbed onto halite surfaces, the composition of crystals is more like brines.

7. Conclusions

In the Dead Sea brines, atmospheric dust particles delivered from surrounding deserts are mainly dissolved in the shallowest water layers and REE released there involved in the halite crystallisation for most part of the year. Accordingly, the dust dissolution corresponds to the REE 'extraction' from the atmospheric dust representing the primary source of these elements, whereas the halite crystallisation corresponds to the formation of a secondary deposit where REE are progressively scavenged. During the dissolution of dust particles, Dead Sea brines inherit their REE distribution characteristic of a shale-like feature in normalised patterns. During the halite crystallisation, the REE partition is constrained by the ionic radius of elements along the REE series. Hence, halite results enriched in MREE and weakly in HREE, whereas La and other LREE remain preferentially partitioned in the coexisting mother brines. These findings suggest a reactor role for the Dead Sea that can extract REE from their primary source accumulating them in a more soluble secondary deposit.

CRediT authorship contribution statement

Conceptualisation: Paolo Censi, Nadav G. Lensky, Ido Sirota, Pierpaolo Zuddas.

Data curation: Marianna Cangemi, Daniela Piazzese.

Formal analysis: Crouvi Onn, Nadav G. Lensky, Ido Sirota, Paolo Censi, Pierpaolo Zuddas.

Funding acquisition: Paolo Censi, Daniela Piazzese, Nadav G. Lensky, Ido Sirota.

Methodology and chemical analysis: Marianna Cangemi, Daniela Piazzese.

Writing: Crouvi Onn, Nadav G. Lensky, Ido Sirota, Paolo Censi, Pierpaolo Zuddas.

Review and editing: Paolo Censi, Daniela Piazzese, Crouvi Onn, Nadav G. Lensky, Ido Sirota, Paolo Censi, Pierpaolo Zuddas.

Data availability

Data will be made available on request.

Declaration of competing interest

We wish to confirm that there are no known conflicts of interest associated with this publication and there has been no significant financial support for this work that could have influenced its outcome.

Acknowledgment

We thank Taglit R/V team – Shahar Gan-El, Meir Yifrach, and Ziv Mor for field assistance. This study was funded by the Israel Science Foundation, PI-NGL (grant # ISF 1471/18), the US-Israel Binational Science Foundation (BSF) Prof. Rahamimoff Travel Grant for Young Scientists to IS (grant # 0378745) and the University of Palermo (CON 0037).

Appendix A. Supplementary data

Supplementary data to this article can be found online at https://doi.org/10.1016/j.scitotenv.2023.162682.

References

Al-Hanbali, A., Kondoh, A., 2008. Groundwater vulnerability assessment and evaluation of human activity impact (HAI) within the Dead Sea groundwater basin,Jordan. Hydrogeol. J. 16, 499–510.

Alibo, D.S., Nozaki, Y., 1999. Rare earth elements in seawater: particle association, shale-normalization, and Ce oxidation. Geochim. Cosmochim. Acta 63, 363–372.

Anati, D.A., 1993. How much salt precipitates from the brines of a hypersaline lake? The Dead Sea as a case study. Geochim. Cosmochim. Acta 57, 2191–2196. https://doi.org/10.1016/0016-7037(93)90560-J.

Arnon, A., Selker, J.S., Lensky, N.G., 2016. Thermohaline stratification and double diffusion diapycnal fluxes in the hypersaline Dead Sea. Limnol. Oceanogr. 61, 1214–1231.

Bąbel, M., Schreiber, B.C., 2014. Geochemistry of evaporites and evolution of seawater. Treatise on Geochemistry, Second edition9, pp. 483–560.

Bau, M., 1996. Controls on the fractionation of isovalent trace elements in magmatic and aqueous systems: evidence from Y/Ho, Zr/Hf, and lanthanide tetrad effect. Contrib. Mineral. Petrol. 123, 323–333.

Bau, M., Dulski, P., 1996. Anthropogenic origin of positive gadolinium anomalies in river waters. Earth Plan. Sci. Lett. 143, 245–255.

Bau, M., Dulski, P., 1999. Comparing yttrium and rare earths in hydrothermal fluids from the Mid-Atlantic Ridge: implications for Y and REE behaviour during near-vent mixing and for the Y/Ho ratio of Proterozoic seawater. Chem. Geol. 155, 77–90.

Belmaker, R., Lazar, B., Stein, M., Taha, N., Bookman, R., 2019. Constraints on aragonite precipitation in the Dead Sea from geochemical measurements of flood plumes. Quat. Sci. Rev. 221, 105876.

Bodaker, I., Sharon, I., Suzuki, M.T., Feingersch, R., Shmoish, M., Andreishcheva, E., et al., 2010. Comparative community genomics in the Dead Sea: an increasingly extreme environment. ISME J. 4, 399–407.

Censi, P., Spoto, S.E., Nardone, G., Saiano, F., Punturo, R., Di Geronimo, S.I., Mazzola, S., Bonanno, A., Patti, B., Sprovieri, M., Ottonello, D., 2005. Rare-earth elements and yttrium distributions in mangrove coastal water systems: The western Gulf of Thailand. Chem. Ecol. 21, 255–277.

Censi, P., Zuddas, P., Larocca, D., Saiano, F., Placenti, F., Bonanno, A., 2007. Recognition of water masses according to geochemical signatures in the Central Mediterranean sea: Y/Ho ratio and rare earth element behaviour. Chem. Ecol. 23 (2), 139–153.

Censi, P., Inguaggiato, C., Chiavetta, S., Schembri, C., Sposito, F., Censi, V., et al., 2017. The behaviour of zirconium, hafnium and rare earth elements during the crystallisation of halite and other salt minerals. Chem. Geol. 453, 80–91.

Censi, P., Sposito, F., Inguaggiato, C., Zuddas, P., Inguaggiato, S., Venturi, M., 2018. Zr, Hf and REE distribution in river water under different ionic strength conditions. Sci. TotalEnviron. 645, 837–853.

Censi, P., Raso, M., Saiano, F., Zuddas, P., Oliveri, E., 2019. Zr/Hf ratio and REE behaviour: A coupled indication of lithogenic input in marginal basins and deep-sea brines. Deep-Sea Res. II Top. Stud. Oceanogr. 164, 216–223.

Censi, P., Sirota, I., Zuddas, P., Lensky, N., Merli, M., Saiano, F., et al., 2020. Trace element fractionation through halite crystallisation: geochemical mechanisms and environmental implications. Sci. Total Environ. https://doi.org/10.1016/j.scitotenv.2020.137926.

Comin-Chiaramonti, P., Civetta, L., Petrini, R., Piccirillo, E.M., Bellieni, G., Censi, P., Bitschene, P., Demarchi, G., De Min, A., Gomes, C.D.E., Castillo, A.M., 1991. Tertiary nephelinitic magmatism in eastern Paraguay: petrology, Sr-Nd isotopes and genetic relationships with associated spinel-peridotite xenoliths. Eur. J. Mineral. 3, 507–525.

Cotton, S., 2006. Lanthanide and Actinide Chemistry. Wiley, pp. 1–263.

Ding, S., Liang, T., Zhang, C., Huang, Z., Xie, Y., Chen, T., 2006. Fractionation mechanisms of rare earth elements (REEs) in hydroponic wheat: an application for metal accumulation by plants. Environ. Sci. Technol. 40, 2686–2691.

Doerner, H.A., Hoskins, W.M., 1925. Coprecipitation of radium and barium sulfates. J. Am. Chem. Soc. 47, 662–675.

Eyal, H., Enzel, Y., Meiburg, E., Vowinckel, B., Lensky, N.G., 2021. How does coastal gravel get sorted under stormy longshore transport? Geophys.Res. Lett. 48, e2021GL095082.

Ganor, E., Foner, H., 2001. Mineral dust concentrations, deposition fluxes and deposition velocities in dust episodes over Israel. Geophys. Res. 106 (D16), 18431–18437.

Ganor, J., Katz, A., 1989. The geochemical evolution of halite structures in hypersaline lakes: The Dead Sea, Israel. Limnol. Oceanogr. 34, 1214–1223.

Gavrieli, I., 1997. Halite deposition from the Dead Sea: 1960–1993. In: Niemi, T.M., Ben-Avraham, Z., Gat, J.R. (Eds.), The Dead Sea, the Lake and Its Setting. Monographs on Geology and Geophysics. 36. Oxford University Press, New York, pp. 161–170.

Gavrieli, I., Halicz, L., 2002. Limnological changes in depth distributions of uranium and rare earth elements in a hypersaline brine: the Dead Sea. Isr. J. Earth Sci. 5, 243–251.

Geng, Y., Cui, D., Yang, L., Xiong, Z., Pavlostathis, S.G., Shao, P., Zhang, Y., Luo, X., Luo, S., 2022. Resourceful treatment of harsh high-nitrogen rare earth element tailings (REEs) wastewater by carbonate activated Chlorococcum sp.microalgae. J. Hazard Mater. 423, 127000.

Goldschmidt, V.M., 1937. The principles of distribution of chemical elements in minerals and rocks. J. Chem. Soc. (Resumed) 655–673.

Goldsmith, Y., Stein, M., Enzel, Y., 2014. From dust to varnish: geochemical constraints on rock varnish formation in the Negev Desert,Israel. Geochim. Cosmochim. Acta 2014 (126), 97–111.

Gwenzi, W., Mangori, L., Danha, C., Chaukura, N., Dunjana, N., Sanganyado, E., 2018. Sources, behaviour, and environmental and human health risks of high-technology rare earth elements as emerging contaminants. Sci. Total Environ. 636, 299–313. https://doi.org/10.1016/j.scitotenv.2018.04.235.

Hao, X., Wang, D., Wang, P., Wang, Y., Zhou, D., 2015. Evaluation of water quality in surface water and shallow groundwater: a case study of a rare earth mining area in southern Jiangxi Province, China. Environ. Monit. Assess. 188 (1), 24.v. https://doi.org/10.1007/s10661-015-5025-1.

Herut, B., Gavrieli, I., Halicz, L., 1998. Coprecipitation of trace and minor elements in modern authigenic halites from the hypersaline Dead Sea brine. Geochim. Cosmochim. Acta 62, 1587–1598.

Jochum, K.P., Seufert, H.M., Spettel, B., Palme, H., 1986. The solar-system abundances of Nb, Ta, and Y, and the relative abundances of refractory lithophile elements in differentiated planetary bodies. Geochim. Cosmochim. Acta 50, 1173–1183.

Kagi, H., Dohmoto, Y., Takano, S., Masuda, A., 1993. Tetrad effect in lanthanide partitioning between calcium sulfate crystal and its saturated solution. Chem. Geol. 107, 71–82.

Kalderon-Asael, B., Erel, Y., Sandler, A., Dayan, U., 2009. Mineralogical and chemical characterization of suspended atmospheric particles over the east Mediterranean based on synoptic-scale circulation patterns. Atmos. Environ. 43, 3963–3970.

Kirkham, C., Bertoni, C., Cartwright, J., Lensky, N.G., Sirota, I., Rodriguez, K., et al., 2020. The demise of a 'salt giant' driven by uplift and thermal dissolution. Earth Plan. Sci. Lett. 531, 115933.

Kulaksiz, S., Bau, M., 2007. Contrasting behaviour of anthropogenic gadolinium and natural rare earth elements in estuaries and the gadolinium input into the North Sea. Earth Plan. Sci. Lett. 260, 361–371.

Kulaksiz, S., Bau, M., 2011. Rare earth elements in the Rhine River, Germany: first case of anthropogenic lanthanum as a dissolved microcontaminant in the hydrosphere. Environ. Int. 37, 973–979.

Kulaksiz, S., Bau, M., 2013. Anthropogenic dissolved and colloid/nanoparticle-bound samarium, lanthanum and gadolinium in the Rhine River and the impending destruction of the natural rare earth element distribution in rivers. Earth Plan. Sci. Lett. 362, 43–50.

Lemaitre, N., Bayon, G., Ondr´eas, H., Caprais, J.C., Freslon, N., Bollinger, C., et al., 2014. Trace element behaviour at cold seeps and the potential export of dissolved iron to the ocean. Earth Planet. Sci. Lett. 404, 376–388.

Lensky, N.G., Dvorkin, Y., Lyakhovsky, V., Gertman, I., Gavrieli, I., 2005. Water, salt, and energy balances of the Dead Sea. Water Res. Res. 41 (12).

Lensky, N.G., Lensky, I.M., Peretz, A., Gertman, I., Tanny, J., Assouline, S., 2018. Diurnal course of evaporation from the Dead Sea in summer: a distinct double peak induced by solar radiation and night sea breeze. Water Resour. Res. 54, 150–160.

Levy, Y., 1992. Modern Sedimentation in the Dead Sea, 1982-1989, Geological Survey of Israel Report Tech. Prog. Rep. (TR-GSI/7/92, 9 pp).

Li, C., 2011. The generalization and application of new technology on lixiviating mineral at the original place for ionic rare earths. Nonferrous Met. Sci. Eng. 2 (1), 63–67. https://doi.org/10.13264/j.cnki.ysjskx.2011.01.007.

Löble, M.W., Keith, J.M., Altman, A.B., Stieber, S.C.E., Batista, E.R., Boland, K.S., Conradson, S.D., Clark, D.L., Lezama Pacheco, J., Kozimor, S.A., Martin, R.L., Minasian, S.G., Olson, A.C., Scott, B.L., Shuh, D.K., Tyliszczak, T., Wilkerson, M.P., Zehnder, R.A., 2015. Covalency in lanthanides. An X-ray absorption spectroscopy and density functional theory study of LnCl6x- (x = 3, 2). J. Am. Chem. Soc. 137, 2506–2523.

Lukens, W.W., Speldrich, M., Yang, P., Duignan, T.J., Autschbach, J., Kögerler, P., 2016. The roles of 4f- and 5f-orbitals in bonding: a magnetochemical, crystal field, density functional theory, and multi-reference wavefunction study. Dalton Trans. 2016 (45), 11508–11521.

Macholdt, D.S., Jochum, K.P., Pohlker, C., Stoll, B., Weis, U., Weber, B., et al., 2015. Microanalytical methods for in-situ high-resolution analysis of rock varnish at the micrometer to nanometer scale. Chem. Geol. 2015 (411), 57–68.

Macholdt, D.S., Jochum, K.P., Pohlker, C., Arangio, A., Forster, J.D., Stoll, B., et al., 2017. Characterization and differentiation of rock varnish types from different environments by microanalytical techniques. Chem. Geol. 459, 91–118.

Migaszewski, Z.M., Gałuszka, A., 2015. The characteristics, occurrence and geochemical behavior of rare earth elements in the environment: a review. Crit. Rev. Environ. Sci. Tech. 45, 429–471. https://doi.org/10.1080/10643389.2013.866622.

Möller, P., Dulski, P., Bau, M., Knappe, A., Pekdeger, A., Sommer-Von Jarmersted, C., 2000. Anthropogenic gadolinium as a conservative tracer in hydrology. J. Geochem. Explor. 69–70, 409–414.

Mor, Z., Assouline, S., Tanny, J., Lensky, I.M., Lensky, N.G., 2018. Effect of water surface salinity on evaporation: the case of a diluted buoyant plume over the Dead Sea. Water Resour. Res. 54, 1460–1475.

Nehorai, R., Lensky, I.M., Hochman, L., Gertman, I., Brenner, S., Muskin, A., Lensky, N.G., 2013. Satellite observations of turbidity in the Dead Sea. J. Geophys. Res. Oceans 118. https://doi.org/10.1002/jgrc.20204.

Palchan, D., Erel, Y., Stein, M., 2018. Geochemical characterization of contemporary fine detritus in the Dead Sea watershed. Chem. Geol. 2018 (494), 30–42.

Penn, R.L., Zhu, C., Xu, H., Veblen, D.R., 2001. Iron oxide coatings on sand grains from the Atlantic coastal plain: High-resolution transmission electron microscopy characterization. Geology 29, 843–846.

Qu, C.L., Liu, G., Zhao, Y.F., 2009a. Experimental study on the fractionation of yttrium from holmium during the coprecipitation with calcium carbonates in seawater solutions. Geochem. J. 43, 403–414.

Qu, C.L., Lu, B., Liu, G., 2009b. Enrichment of lanthanides in aragonite. J. Rare Earths 27, 1062–1065.

Raso, M., Censi, P., Saiano, F., 2013. Simultaneous determinations of zirconium, hafnium, yttrium and lanthanides in seawater according to a co-precipitation technique onto iron-hydroxide. Talanta 116, 1085–1090.

Rouchy, J.M., Caruso, A., 2006. The Messinian salinity crisis in the Mediterranean basin: a reassessment of the data and an integrated scenario. Sediment. Geol. 188–189, 35–67.

Ruberti, E., Castorina, F., Censi, P., Comin-Chiaramonti, P., Gomes, C.B., Antonini, P., Andrade, F.R.D., 2002. The geochemistry of the Barra do Itapirapuã carbonatite (Ponta Grossa Arch, Brazil): a multiple stockwork. J. South Am. Earth Sci. 15, 215–228.

Salhotra, A.M., Adams, E.E., Harleman, D.R.F., 1987. The alpha, beta, gamma of evaporation from saline water bodies. Water Resour. Res. 23, 1769–1774.

Shannon, R.D., 1976. Revised effective ionic radii and systematic studies of interatomic distances in halides and chalcogenides. Acta Crystallogr.Sect.A 32, 751–767.

Singer, A., Ganor, E., Dultz, S., Fischer, W., 2003. Dust deposition over the Dead Sea. J. Arid Environ. 53, 41–59.

Sirota, I., Arnon, A., Lensky, N.G., 2016. Seasonal variations of halite saturation in the Dead Sea. Water Res. Res. 52, 7151–7162.

Sirota, I., Enzel, Y., Lensky, N.G., 2017. Temperature seasonality control on modern halite layers in the Dead Sea: in situ observations. Geol. Soc. Am. Bull. 129, 1181–1194.

Sirota, I., Enzel, Y., Lensky, N.G., 2018. Halite focusing and amplification of salt layer thickness: from the Dead Sea to deep hypersaline basins. Geology 2018 (46), 851–854.

Sirota, I., Ouillon, R., Mor, Z., Meiburg, E., Enzel, Y., Arnon, A., Lensky, N.G., 2020. Hydroclimatic controls on salt fluxes and halite deposition in the Dead Sea and the shaping of "salt giants". Geophys. Res. Lett. 47, e2020GL090836.

Sirota, I., Enzel, Y., Mor, Z., Ben Moshe, L., Eyal, H., Lowenstein, T.K., Lensky, N.G., 2021. Sedimentology and stratigraphy of a modern halite sequence formed under Dead Sea level fall. Sedimentology 68, 1069–1090.

Steinhorn, I., 1983. In situ salt precipitation at the Dead Sea. Limnol.Oceanogr. 28, 580–583.

Takahashi, Y., Châtellier, X., Hattori, K.H., Kato, K., Fortin, D., 2005. Adsorption of rare earth elements onto bacterial cell walls and its implication for REE sorption onto natural microbial mats. Chem. Geol. 219, 53–67.

Takahashi, Y., Hirata, T., Shimizu, H., Ozaki, T., Fortin, D., 2007. A rare earth element signature of bacteria in natural waters? Chem. Geol. 244, 569–583.

Takahashi, Y., Yamamoto, M., Yamamoto, Y., Tanaka, K., 2010. EXAFS study on the cause of enrichment of heavy REEs on bacterial cell surfaces. Geochim. Cosmochim. Acta 74, 5443–5462.

Taylor, S.R., McLennan, S.M., 1985. The continental crust: its composition and evolution. An Examination of the Geochemical Record Preserved in Sedimentary Rocks. Blackwell.

Terakado, Y., Masuda, A., 1988. The coprecipitation of rare-earth elements with calcite and aragonite. Chem. Geol. 69, 103–110.

Thiagarajan, N., Lee, CTA., 2004. Trace-element evidence for the origin of desert varnish by direct aqueous atmospheric deposition. Earth Plan. Sc. Lett. 224, 131–141.

Warren, J.K., 2006. Evaporites: Sediments, Resources and Hydrocarbons. Springer, pp. 1–1035.

Wilfong, W.C., Ji, T., Duan, Y., Shi, F., Wang, Q., Gray, M.L., 2022. Critical review of functionalized silica sorbent strategies for selective extraction of rare earth elements from acid mine drainage. J.Hazard. Mater. 424, 127625.